Plasmons in molecules: Microscopic characterization based on orbital transitions and momentum conservation

Caroline M. Krauter,[1,2,a)] Jochen Schirmer,[1] Christoph R. Jacob,[3] Markus Pernpointner,[1] and Andreas Dreuw[2]

[1]*Theoretical Chemistry, Heidelberg University, Im Neuenheimer Feld 229, D-69120 Heidelberg, Germany*
[2]*Interdisciplinary Center for Scientific Computing, Heidelberg University, Im Neuenheimer Feld 368, 69120 Heidelberg, Germany*
[3]*Center for Functional Nanostructures and Institute of Physical Chemistry, Karlsruhe Institute of Technology (KIT), Wolfgang-Gaede-Strasse 1a, 76131 Karlsruhe, Germany*

(Received 13 June 2014; accepted 19 August 2014; published online 8 September 2014)

In solid state physics, electronic excitations are often classified as plasmons or single-particle excitations. The former class of states refers to collective oscillations of the electron density. The random-phase approximation allows for a quantum-theoretical treatment and a characterization on a microscopic level as a coherent superposition of a large number of particle-hole transitions with the same momentum transfer. However, small systems such as molecules or small nanoclusters lack the basic properties (momentum conservation and uniform exchange interaction) responsible for the formation of plasmons in the solid-state case. Despite an enhanced interest in plasmon-based technologies and an increasing number of studies regarding plasmons in molecules and small nanoclusters, their definition on a microscopic level of theory remains ambiguous. In this work, we analyze the microscopic properties of molecular plasmons in comparison with the homogeneous electron gas as a model system. Subsequently, the applicability of the derived characteristics is validated by analyzing the electronic excitation vectors with respect to orbital transitions for two linear polyenes within second order versions of the algebraic diagrammatic construction scheme for the polarization propagator.
 [http://dx.doi.org/10.1063/1.4894266]

I. INTRODUCTION

Over the past few decades, plasmonics has evolved as a promising field of research. The term plasmons refers to collective oscillations of the valence electron gas in conducting materials like metals, metal nanoclusters, or graphene. Due to their high absorption cross sections plasmons usually dominate the optical properties of such materials, which in combination with efficient energy and information transport make plasmons interesting targets for the field of electronics, e.g., as chemical or biological sensors,[1–3] photovoltaic devices,[4,5] metamaterials[6–9] or high frequency computer chips.[10–13] They have also been used in photocatalytic redox reactions.[14–17]

In an extended system, such as the degenerate electron gas, plasmon excitations can be treated as macroscopic electron density waves using classical electrodynamics. The random phase approximation (RPA) allows for a quantum-theoretical treatment of plasmons,[18–22] reproducing the classical result for the plasmon frequency in the long-wavelength limit. In the microscopic description according to the RPA, a plasmon emerges as a coherent superposition of a large number of elementary particle-hole (p-h) excitations, comprising all elementary excitations with a given momentum transfer. A dominant uniform exchange interaction of the elementary p-h excitations is crucial in forming such collective excitations.

Plasmon excitations have been postulated to arise also in smaller systems exhibiting molecular-type electronic structures, e.g., in metal clusters with dimensions of about 2 nm or even less,[23–26] or in organic molecules such as polyacenes and fullerenes.[27–33] However, the question arises how collective excitations could possibly emerge in systems lacking the essential features of the solid-state case, such as momentum conservation and a preeminent uniform exchange interaction. Nevertheless, various theoretical studies have been performed addressing plasmon-type optical excitations in small metal clusters (e.g., Refs. 24, 34–42) and molecules (e.g., Refs. 33, 43–52). Most of these studies are based on applications of TDDFT methods[53–55] or the RPA.

It should be noted that the concept of plasmon excitations in small clusters and molecules is by no means unchallenged. For example, it has been argued that there are no plasmon-type excitations in small clusters and molecules.[56] While a valid approach was used to analyze the computed excitation manifold with regard to possible plasmon-type features, some of the conclusions seem to be unsubstantiated. By contrast, quantum fluid dynamics and TDDFT simulations have shown that certain microscopic electronic excitations can indeed be correlated with collective oscillations, even in very small systems like Na_2.[57,58] Finally, one of us has recently demonstrated by comparison to the electron gas that the notion of a plasmon can indeed be transferred to molecular systems.[59]

While the microscopic quantum-theoretical treatment based on the RPA or TDDFT methods provide for the pertinent information on the respective excited states, i.e.,

a)Present address: Department of Mechanical and Aerospace Engineering, Princeton University, Princeton, New Jersey 08544-5263, USA. Electronic mail: Caroline.Krauter@pci.uni-heidelberg.de.

energies, transition moments, and eigenvector components, a clear and comprehensive definition of what constitutes a plasmon in a small system is still wanting. Often, the term plasmon is simply attributed to a state having a large spectral intensity; or to a state characterized as a linear combination of a few elementary p-h excitations, interpreted as signature of collective character. More rigorously, Bernadotte *et al.* derived a scaling approach for TDDFT methods to differentiate between plasmons and single-particle transitions in a broad range of molecular systems.[59] It is based on the different dependence of the energy of single-particle excitations and plasmons on the electron-electron interaction. Such an analysis has subsequently been applied also by other authors.[33,42]

In the present paper we will review the theory of plasmons, addressing in particular its implications for molecules and small clusters. To complement the previous work by Bernadotte *et al.*,[59] we will focus on the characterization of the eigenvector components of the states associated with plasmons. Recalling the RPA treatment of electronic excitations in the degenerate electron gas, the plasmon features established there will be transferred to the analysis and characterization of low-lying excitations of two polyene molecules. Although the treatment of electronic excitations in the electron gas by the RPA has nowadays become textbook knowledge,[22,60] a brief review will be given here as its understanding is a necessary prerequisite for an unfamiliar reader to follow our line of argumentation. Moreover, we will use a formulation in terms of the polarization propagator here in order to make the connection to quantum chemical wavefunction methods for the calculation of excited states possible.

This work is organized as follows. In Sec. II an overview over the theory of plasmons within the RPA is given. The results for the linear polyenes octatetraene (C_8H_{10}) and $C_{16}H_{18}$ are presented in Sec. III.

II. PLASMON EXCITATIONS IN AN ELECTRON GAS

A uniform gas of electrons, for electric neutrality embedded in a continuous positive background, responds to a perturbation of the equilibrium electron density by density oscillations, also referred to as plasma oscillations. Being a macroscopic phenomenon, these oscillations can be treated within the framework of classical mechanics and electrodynamics.[22,61]

A well-known approach to electronic excitation is the RPA. Applied to the electron gas, a plasmon solution is found, the frequency being identical with the classical result (in the limit of large wavelengths). Below, we will review the RPA treatment of the electron gas.

A. The homogeneous electron gas

In the following, we consider a homogeneous electron gas enclosed in a box with volume $\mathcal{V} = L^3$ with periodic boundary conditions as a model for a metal and assume a uniform positively charged background. Neglecting any interaction between the electrons, the single-particle states (spin orbitals) $\psi_{\mathbf{k}\sigma}$ are obtained as products between a spatial orbital $\phi_{\mathbf{k}}$ and a spin function $\gamma(s)$,

$$\psi_{\mathbf{k}\gamma}(\mathbf{x}, s) = \phi_{\mathbf{k}}(\mathbf{x})\gamma(s) = \frac{1}{\sqrt{\mathcal{V}}} e^{i\mathbf{k}\mathbf{x}}\gamma(s), \quad \gamma \in \{\alpha, \beta\}. \tag{1}$$

Here, $\mathbf{x}$ denotes the Cartesian coordinates and s the spin coordinate. The spatial orbitals are plane-waves characterized by the wave vectors $\mathbf{k}$. Using the periodic boundary conditions, their components are given by

$$k_i = \frac{2\pi n_i}{L} \quad (i = x, y, z,\ n_i = 0, \pm 1, \pm 2, \dots). \tag{2}$$

The wave vectors are also referred to as momentum vectors. The single-particle (orbital) energies $\epsilon_{\mathbf{k}}$ are

$$\epsilon_{\mathbf{k}} = \frac{\hbar^2 |\mathbf{k}|^2}{2m_e}. \tag{3}$$

For $\mathcal{V} \to \infty$ the wave vectors can be treated as being continuous. In the ground state of a system containing N electrons, the N energetically lowest spin orbitals are occupied. The energy of the highest orbital is called Fermi energy ϵ_F. The corresponding Fermi wave number (also called Fermi momentum) k_F can be used to define occupation numbers $n_{\mathbf{k}}$,

$$n_{\mathbf{k}} = \Theta(k_F - |\mathbf{k}|) = \begin{cases} 0, & |\mathbf{k}| > k_f \\ 1, & |\mathbf{k}| \le k_f \end{cases}. \tag{4}$$

B. Linear response to an external perturbation and the polarization propagator

In linear response theory the density change induced by an external potential is described by the time-space integral over the product of the retarded density correlation function $D^R(\mathbf{x}, \mathbf{x}')$ and the external potential $\Phi_{ext}(\mathbf{x}, t)$.[22] To allow one to evaluate the correlation function in perturbation theory, it is convenient to define an associated time-ordered correlation function which then contains the same physical information.[22] Here, we will use the polarization propagator $\Pi(\mathbf{x}t, \mathbf{x}'t')$. Fourier transformation from the space domain into the momentum domain and from the time domain to the frequency domain as well as insertion of a complete set of eigenstates of $\hat{H}$ leads to the well-known spectral or Lehmann representation of the polarization propagator,[22]

$$\Pi_{pr,p'r'}(\omega) = \underbrace{\sum_{m\neq 0} \frac{\langle\Psi_0|c_r^\dagger c_p|\Psi_m\rangle\langle\Psi_m|c_{p'}^\dagger c_{r'}|\Psi_0\rangle}{\omega - (E_m - E_0) + i\eta}}_{\Pi^+_{pr,p'r'}(\omega)} + \underbrace{\sum_{m\neq 0} \frac{\langle\Psi_0|c_{p'}^\dagger c_{r'}|\Psi_m\rangle\langle\Psi_m|c_r^\dagger c_p|\Psi_0\rangle}{\omega + (E_m - E_0) - i\eta}}_{\Pi^-_{pr,p'r'}(\omega)}. \tag{5}$$

Here, the indices p and r denote spin-orbitals,

$$p \equiv \mathbf{j}\tau \quad \text{and} \quad r \equiv \mathbf{k}\sigma. \tag{6}$$

The factors $\pm i\eta$ guarantee convergence of the Fourier transformations. The poles of $\Pi_{pr,p'r'}(\omega)$ determine the excitation energies of the states that are coupled to the ground state *via* the density operator.

The two terms of the matrix $\mathbf{\Pi}(\omega)$, denoted as $\mathbf{\Pi}^{+}(\omega)$ and $\mathbf{\Pi}^{-}(\omega)$, both contain the same physical information. The poles of the first term $\mathbf{\Pi}^{+}(\omega)$ correspond to excitation energies (p-h states) while those of $\mathbf{\Pi}^{-}(\omega)$, referred to as deexcitations (h-p states), are the negative excitation energies. They are connected by

$$\Pi^{+}_{pr,p'r'}(\omega) = \Pi^{-}(-\omega)_{r'p',rp}. \tag{7}$$

To compute the polarization propagator one has to resort to suitable approximation schemes. Here a central role is played by the RPA to be addressed in the following.

C. Random-phase approximation

The RPA was first derived by Pines and Bohm.[18–21] They used an effective screened Coulomb force, among other approximations, to separate collective modes (plasmons) from single-particle excitations. The resulting quantum mechanical description of plasmons constitutes one of the greatest successes of the RPA.

Within the RPA approximation, the polarization propagator is given by

$$\Pi^{RPA}_{pr,p'r'}(\omega) = \Pi^{0}_{pr,p'r'}(\omega) + \Pi^{0}_{pr,pr}(\omega) \sum_{p''r''} U_{pr,p''r''}\, \Pi^{RPA}_{p''r'',p'r'}(\omega). \tag{8}$$

Here, $\Pi^{0}_{pr,p'r'}(\omega)$ is the zeroth order (diagonal) polarization propagator and with the non-interacting homogeneous electron gas as a reference,

$$\Pi^{0}_{pr,p'r'}(\omega) = \left[\frac{(1-n_p)n_r}{\omega+\epsilon_r-\epsilon_p+i\eta} - \frac{n_p(1-n_r)}{\omega+\epsilon_r-\epsilon_p-i\eta}\right]\delta_{rr'}\delta_{pp'}, \tag{9}$$

with ϵ_p and n_r being the single-particle energies and occupation numbers as defined above. The quantities $U_{rp,r'p'}$ are elements of the interaction matrix and have the following form:

$$U_{pr,p'r'} = -V_{pr'[p'r]} = -\langle pr'||p'r\rangle = -\langle pr'|p'r\rangle + \langle pr'|rp'\rangle. \tag{10}$$

This is the RPA as commonly used in quantum chemistry. In solid state physics, this expression is usually further approximated by neglect of the Coulomb type term $(-\langle pr'|p'r\rangle)$ because the exchange term dominates for small $\mathbf{q}$:

$$U_{pr,p'r'} = V_{pr'rp'} = \langle pr'|rp'\rangle. \tag{11}$$

This additional approximation is discussed in more detail in Sec. II of the supplementary material.[62] Here we adopt this approach and only work with the latter definition given in Eq. (11).

The RPA equations decouple into separate equations for singlet and triplet excitations, which can be achieved by applying suitable unitary transformations. The general form of the RPA equations is as given by Eq. (8), the respective spin-free interaction matrix elements reading

$${}^{S}U_{\mathbf{jk},\mathbf{j'k'}} = 2V_{\mathbf{jk'kj'}}, \quad {}^{T}U_{\mathbf{jk},\mathbf{j'k'}} = 0. \tag{12}$$

Consequently, the triplet states do not include any interaction between different p-h excitations and at this level of approximation their excitation energies are given directly by orbital energy differences of the non-interacting reference system.

With this approximate electron-electron interaction the singlet part of the spin-adapted polarization propagator can be written as

$${}^{S}\Pi^{RPA}_{\mathbf{jk},\mathbf{j'k'}}(\omega) = {}^{S}\Pi^{0}_{\mathbf{jk},\mathbf{j'k'}}(\omega) + {}^{S}\Pi^{0}_{\mathbf{jk},\mathbf{jk}}(\omega) \sum_{\mathbf{j''k''}} {}^{S}U_{\mathbf{jk},\mathbf{j''k''}}\, {}^{S}\Pi^{RPA}_{\mathbf{j''k''},\mathbf{j'k'}}(\omega). \tag{13}$$

We will continue working with the singlet expressions only. Therefore, the superscript S will be dropped and singlet symmetry implicitly assumed.

The matrix $\mathbf{\Pi}^{0}(\omega)$ is the zeroth order polarization propagator and for the non-interacting homogeneous electron gas as reference its matrix elements are given by

$$\Pi^{0}_{\mathbf{jk},\mathbf{j'k'}}(\omega) = \left[\frac{(1-n_\mathbf{j})n_\mathbf{k}}{\omega+\epsilon_\mathbf{k}-\epsilon_\mathbf{j}+i\eta} - \frac{n_\mathbf{j}(1-n_\mathbf{k})}{\omega+\epsilon_\mathbf{k}-\epsilon_\mathbf{j}-i\eta}\right]\delta_{\mathbf{kk'}}\delta_{\mathbf{jj'}}. \tag{14}$$

The two-electron integrals as occurring in the expression for the interaction can be readily evaluated yielding[22]

$$V_{\mathbf{jk'kj'}} = \frac{4\pi e^2}{\mathcal{V}}\frac{1}{(\mathbf{j}-\mathbf{k})^2}\delta_{\mathbf{j}+\mathbf{k'},\mathbf{j'}+\mathbf{k}}. \tag{15}$$

The detailed derivation is given in the supplementary material.[62]

At this point, momentum conservation comes into play and renders one of the four indices redundant. By defining the momentum transfer $\mathbf{q} \equiv \mathbf{j}-\mathbf{k} = \mathbf{j'}-\mathbf{k'}$ and subsequently writing $\mathbf{j} = \mathbf{k}+\mathbf{q}$ as well as $\mathbf{j'} = \mathbf{k'}+\mathbf{q}$ the following expressions are obtained:

$$V_{\mathbf{k},\mathbf{k'}}(\mathbf{q}) \equiv V_{(\mathbf{k}+\mathbf{q})\mathbf{k'}\mathbf{k}(\mathbf{k'}+\mathbf{q})} = \frac{4\pi e^2}{\mathcal{V}}\frac{1}{\mathbf{q}^2} = V(\mathbf{q}). \tag{16}$$

Consequently, $V_{\mathbf{jk'kj'}}$ is solely determined by the momentum transfer $\mathbf{q} = \mathbf{j}-\mathbf{k}$.

As a result of momentum conservation, the polarization propagator depends on only three independent indices, too. The matrix elements of the polarization propagator can hence be rewritten as

$$\Pi^{RPA}_{\mathbf{k},\mathbf{k'}}(\mathbf{q},\omega) = \Pi^{0}_{\mathbf{k},\mathbf{k'}}(\mathbf{q},\omega) + \Pi^{0}_{\mathbf{k},\mathbf{k}}(\mathbf{q},\omega)2V(\mathbf{q}) \sum_{\mathbf{k''}} \Pi^{RPA}_{\mathbf{k''},\mathbf{k'}}(\mathbf{q},\omega). \tag{17}$$

The separation of the polarization propagator with respect to the momentum transfer is a very important result of this discussion. The set of RPA equations are now replaced by a separate set of equations for each value of $\mathbf{q}$. This separability will become important when discussing the character of the plasmon states.

In a compact matrix notation the polarization propagator is given by

$$\mathbf{\Pi}^{RPA}(\mathbf{q},\omega) = \mathbf{\Pi}^{0}(\mathbf{q},\omega) + \mathbf{\Pi}^{0}(\mathbf{q},\omega)\mathbf{U}(\mathbf{q})\mathbf{\Pi}^{RPA}(\mathbf{q},\omega) \tag{18}$$

with the interaction matrix $\mathbf{U}(\mathbf{q})$ being a constant and uniform matrix with elements $U_{\mathbf{k},\mathbf{k}'}(\mathbf{q}) = 2V(\mathbf{q})$. The formal solution

$$\mathbf{\Pi}^{RPA}(\mathbf{q},\omega) = (\mathbf{\Pi}^{0}(\mathbf{q},\omega)^{-1} - \mathbf{U}(\mathbf{q}))^{-1} \tag{19}$$

can be rewritten in the form of the well-known pseudo-eigenvalue equation,

$$\begin{pmatrix} \mathbf{A}(\mathbf{q}) & \mathbf{B}(\mathbf{q}) \\ \mathbf{B}^{*}(\mathbf{q}) & \mathbf{A}^{*}(\mathbf{q}) \end{pmatrix} \begin{pmatrix} \mathbf{x} \\ \mathbf{y} \end{pmatrix} = \omega_n \begin{pmatrix} \mathbf{x} \\ -\mathbf{y} \end{pmatrix},$$

$$\text{with} \quad A_{\mathbf{k},\mathbf{k}'}(\mathbf{q}) = (\epsilon_{\mathbf{k}+\mathbf{q}} - \epsilon_{\mathbf{k}})\delta_{\mathbf{k},\mathbf{k}'} + 2V(\mathbf{q}), \tag{20}$$

$$B_{\mathbf{k},\mathbf{k}'}(\mathbf{q}) = 2V(\mathbf{q}).$$

For each value of $\mathbf{q}$ a separate pseudo-eigenvalue problem is obtained due to the decoupling of single-particle excitations of different momentum transfer. Moreover, single-particle states with the same value for $\mathbf{q}$ interact in a completely uniform way. Of course, this is only the case if the Coulomb term to the interaction is neglected as in Eq. (11).

However, the resulting matrices are extremely large (in the limit $V \to \infty$ infinite) and it is desirable to replace such matrix equations by analytical expressions. The homogeneity of the interaction allows one to write the matrices as $\mathbf{q}$-dependent functions. For this purpose, we define $\Pi^{RPA}(\mathbf{q},\omega) \equiv \sum_{\mathbf{k}\mathbf{k}'} \Pi^{RPA}_{\mathbf{k},\mathbf{k}'}(\mathbf{q},\omega)$. In analogy, we define $\Pi^{0}(\mathbf{q},\omega) \equiv \sum_{\mathbf{k}} \Pi^{0}_{\mathbf{k},\mathbf{k}}(\mathbf{q},\omega)$ and get

$$\begin{aligned} \Pi^{RPA}(\mathbf{q},\omega) &= \Pi^{0}(\mathbf{q},\omega) + \Pi^{0}(\mathbf{q},\omega)2V(\mathbf{q})\Pi^{RPA}(\mathbf{q},\omega) \\ &= \underbrace{(1 - \Pi^{0}(\mathbf{q},\omega)2V(\mathbf{q}))^{-1}}_{\epsilon^{RPA}(\mathbf{q},\omega)}\Pi^{0}(\mathbf{q},\omega), \end{aligned} \tag{21}$$

where $\epsilon^{RPA}(\mathbf{q},\omega)$ is the so-called dielectric function at the RPA level. It describes the modification to the lowest order interaction by the polarization of the medium and can be used to determine several properties like the plasma oscillations or screening effects.[22,61] Determining the poles of the polarization propagator is equivalent to finding the roots of the dielectric function and the following equation has to be solved for the eigenvalues ω_n:

$$1 = \Pi^{0}(\mathbf{q},\omega)2V(\mathbf{q}) \tag{22}$$

with

$$\Pi^{0}(\mathbf{q},\omega) = \sum_{\mathbf{k}} \left[\frac{(1 - n_{\mathbf{k}+\mathbf{q}})n_{\mathbf{k}}}{\omega + \epsilon_{\mathbf{k}} - \epsilon_{\mathbf{q}+\mathbf{k}} + i\eta} - \frac{n_{\mathbf{k}+\mathbf{q}}(1 - n_{\mathbf{k}})}{\omega + \epsilon_{\mathbf{k}} - \epsilon_{\mathbf{k}+\mathbf{q}} - i\eta} \right]. \tag{23}$$

Let us note that in Ref. 59 a distinction between plasmons and (renormalized) single-particle excitations has been introduced based on Eq. (21), because poles of Π^{RPA} can formally arise from poles of Π^{0} or from roots of the dielectric function ϵ^{RPA}. The single-particle states were obtained from Π^{0} and the plasmon solutions were extracted from ϵ^{RPA}. However, the poles of Π^{0} are canceled by poles of the dielectric function (both depending on Π^{0}) and thus become renormalized, with the renormalized states also given as roots of the dielectric function. Consequently, the roots of the dielectric function ϵ^{RPA} give not only plasmons but also the single-particle states.

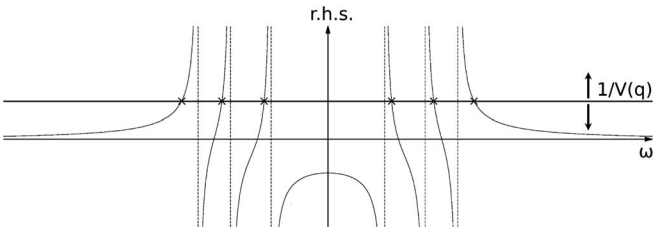

FIG. 1. Exemplary graphical solution of the eigenvalue equation (24). Based on Refs. 22 and 60.

D. Graphical solution of the RPA equations

The eigenvalue equation (22) can be solved graphically by recasting it in the following form:[22,60]

$$\frac{1}{V(\mathbf{q})} = 2\sum_{\mathbf{k}} \left[\frac{(1 - n_{\mathbf{k}+\mathbf{q}})n_{\mathbf{k}}}{\omega + \epsilon_{\mathbf{k}} - \epsilon_{\mathbf{q}+\mathbf{k}}} - \frac{n_{\mathbf{k}+\mathbf{q}}(1 - n_{\mathbf{k}})}{\omega + \epsilon_{\mathbf{k}} - \epsilon_{\mathbf{k}+\mathbf{q}}} \right]. \tag{24}$$

The complex factors $\pm i\eta$ have been dropped because they are not important here. The excitation energies are given by the intersection points between the right-hand side (r.h.s.) of Eq. (24) plotted in dependence of the frequency ω and the line given by the constant function $f(\omega) = \frac{1}{V(\mathbf{q})}$. This is shown schematically for an example with $m = 3$ single-particle replacements $\mathbf{k} \to \mathbf{k} + \mathbf{q}$ for a specific value of $\mathbf{q}$ and the interaction strength $V(\mathbf{q})$ in Figure 1.

As a characteristic feature of the RPA, to each positive excitation energy a negative counterpart exists that corresponds to a deexcitation with the same energy. The poles of the r.h.s correlate with poles of Π^{0} and are thus given by orbital energy differences. Altogether, there are m excitation and deexcitation energies each. Here, we consider only excitations. Of these m energies, $m - 1$ solutions are enclosed between two successive poles of the r.h.s. while the mth and highest state, positioned on the right-hand side of the last pole, is strongly dependent on the interaction strength $V(\mathbf{q})$. This latter state corresponds to a collective state (plasmon) while the other $m - 1$ energetically lower states are ordinary single-particle states. Consequently, when varying $V(\mathbf{q})$, the ordinary single-particle states change only little in energy in contrast to the distinct plasmon solution. Evaluation of the plasmon frequency ω_{pl} reveals that $\omega^{2}_{pl} \propto V(\mathbf{q})$.[22,59,60]

A further simplification *via* the assumption that the orbital energy differences are all equal (with $\epsilon_{\mathbf{j}} - \epsilon_{\mathbf{k}} = \Delta\epsilon \quad \forall \mathbf{j},\mathbf{k}$) allows one to analyze the eigenvectors of the m possible excitations in more detail. Using the pseudo-eigenvalue Eq. (20), the eigenvector $\mathbf{v}_{pl}$ of the plasmon excitation is now given by

$$\mathbf{v}_{pl} = \begin{pmatrix} \mathbf{x}_{pl} \\ \mathbf{y}_{pl} \end{pmatrix} \tag{25}$$

$$\text{with} \quad \mathbf{x}_{pl} = N \begin{pmatrix} 1 \\ 1 \\ \vdots \\ 1 \end{pmatrix} \quad \text{and} \quad \mathbf{y}_{pl} = -\frac{\omega_{pl} - \Delta\epsilon}{\omega_{pl} + \Delta\epsilon} N \begin{pmatrix} 1 \\ 1 \\ \vdots \\ 1 \end{pmatrix},$$

where N is a normalization factor. The eigenvectors for the $(m-1)$ single-particle states can be chosen to be $(l = 1, \ldots, m-1)$

$$\mathbf{v}_l = \begin{pmatrix} \mathbf{x}_l \\ \mathbf{0} \end{pmatrix} \quad \text{with} \quad \mathbf{x}_l \perp \mathbf{x}_{pl} \quad \text{and} \quad |\mathbf{x}_l| = 1,$$

$$\text{e.g.,} \quad \mathbf{x}_i = \frac{1}{\sqrt{2}} \begin{pmatrix} 1 \\ -1 \\ 0 \\ \vdots \\ 0 \end{pmatrix}. \tag{26}$$

In contrast to the single-particle excitations, the plasmon is a positive linear combination of all m possible single-particle replacements with a given momentum transfer $\mathbf{q}$. All single-particle transitions with momentum transfer $\mathbf{q}$ contribute with equal phase and weight. In other words, it is a coherent superposition of all single-particle excitations with a given momentum transfer $\mathbf{q}$. This reflects the collective character of this state.

Let us note that the manifold of elementary excitations constituting a plasmon-type excitation need not to be large. In the case depicted in Figure 1, e.g., there are $m = 3$ elementary excitations giving rise to two ordinary and one plasmon solutions. Even the case $m = 1$ is conceivable and the single solution arising here shows the characteristic plasmon-type behavior with respect to the variation of $V(\mathbf{q})$.

Further evaluation of the transition matrix elements shows that only the plasmonic excitation has a non-zero transition strength.[22,60] In a sense, the plasmon collects the intensity of all the underlying single-particle replacements explaining the high absorption cross sections observed in experiments. These results finally explain how a plasmon differs microscopically from ordinary single-particle excitations.

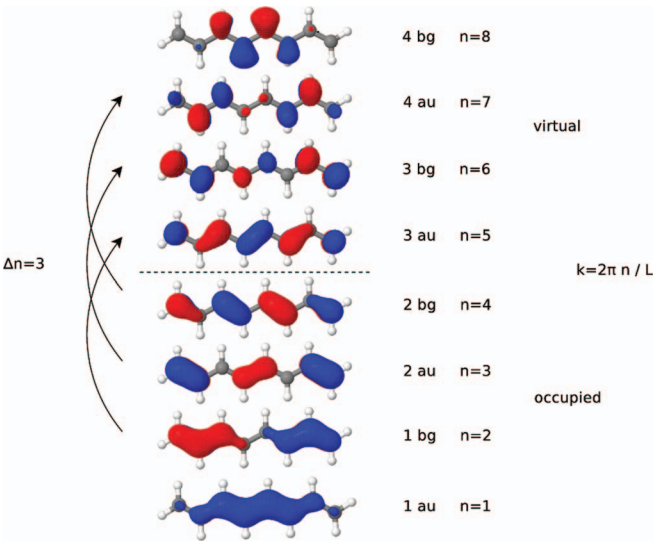

FIG. 2. Molecular orbitals of octatetraene and assignment of momentum vectors k. The symbol n denotes the quantum numbers of the orbitals. As an example, the three arrows indicate the three possible single-particle replacements with $\Delta n = 3$.

Moreover, this behavior is independent of the number of electrons present in the system.

Evaluation of the plasmon frequency ω_{pl} within the approximation of equally spaced single-particle states, yields

$$\omega_{pl} = \Delta\epsilon \left(1 + \frac{2mV(\mathbf{q})}{\Delta\epsilon}\right)^{\frac{1}{2}}. \tag{27}$$

As a consequence, the square of the plasmon frequency depends linearly on the interaction strength ($\omega_{pl}^2 \propto V(\mathbf{q})$) as already mentioned above. The different behavior of the plasmon and single-particle frequencies on the interaction $V(\mathbf{q})$ was also realized in Ref. 59 using a slightly different approach where it was used to establish a scaling approach for the identification of plasmon excitations within the framework of TDDFT.

Plasmons can also be described in the Tamm-Dancoff approximation (TDA),[22] as well referred to as configuration interaction singles (CIS)[63] in the quantum chemistry community. The TDA secular matrix corresponds to the submatrix $\mathbf{A}$ of the RPA secular matrix in Eq. (20). Carrying out a similar graphical analysis as above for RPA, reveals qualitatively the same results. The plasmon state is the highest in energy, depends strongly on the electron-electron interaction, gathers all the intensity, and is a linear combination of all single-particle replacements with the given value of $\mathbf{q}$.

In conclusion, the main characteristic features of the degenerate electron gas, relevant to the issue of plasmon excitations in molecules are the following:

- The momentum transfer is a conserved quantity. As a consequence, the secular problem for excited states decouples with respect to the momentum transfer of the excited states. For a given momentum transfer $\mathbf{q}$, there is only a limited number of elementary excitations, e.g., single-particle excitations, and the corresponding excitation energies lie within a finite range.
- The secular matrix for the single-particle excitations (singlets) is dominated by the exchange contributions, establishing a uniform interaction matrix. Note that this does not apply to triplet excitations.

While the first property here is an indispensable requirement, the presence of a dominant uniform interaction may be of more gradual relevance. One may expect that the non-uniform direct Coulomb contributions in the secular matrix will modify the picture to a certain extent but not alter it completely. This remark should apply also to a treatment taking two-particle and higher excitations into account.

Consequently, the question arises how collective excitations emerge in molecular systems or small nanoclusters, which lack these essential features of the solid-state case. This issue will be analyzed in the following section using two linear polyenes as illustrative examples.

That plasmonic states are build up from linear combinations of several single-particle transitions has been recognized by several authors, e.g., Refs. 51, 56, 64, 65. However, a plausible distinction between ordinary excitations, which as well may be linear combinations of elementary p-h replacements, and plasmon excitations, has not been established

previously. In particular, the crucial role of a symmetry constraint (such as momentum conservation) leading to finite separate manifolds of elementary p-h excitations, has not been addressed.

III. PLASMONS IN LINEAR POLYENES

In the following we will analyze the electronic excitations in the linear polyenes C_8H_{10} and $C_{16}H_{18}$ and validate the presence of plasmon-type excitations exhibiting the microscopic characteristics established in Sec. II D.

In linear polyenes the π electrons can be viewed as forming a quasi one-dimensional electron gas along the molecule (see the π-orbitals shown in Figures 2 and 3). In analogy to the homogeneous one-dimensional electron gas in a box one may assign wave vectors to the Hartree-Fock π-orbitals of the polyenes. While such an assignment of momentum vectors is not rigorous, it provides for a useful qualitative means to classify the p-h excitations and to identify plasmon-type excitations. In the one-dimensional case, the wave vectors have only one component, and a given momentum transfer can be directly correlated to a corresponding change in the quantum numbers of the orbitals involved in the respective p-h transition (compare Figure 2).

It should be noted that the overall phase of a HF orbital is not determined *a priori* and different computations may result in different phases. This has to be taken into account when the final state eigenvectors are to be inspected. The sign of an eigenvector component reflects the orbital phases in the corresponding elementary p-h excitation. Therefore, the orbitals have to be defined in the same way as in the respective particle in a box model in order to evaluate the amplitudes of different p-h transitions as described above.

The linear polyenes have C_{2h} symmetry and the π-orbitals transform according to the irreducible representations A_u or B_g. Therefore, the $\pi\pi^*$ excitations are either of A_g (even change in quantum number) or B_u (odd change in quantum number) symmetry. While excitations of the latter type are optically allowed, the former ones are dark states and have no intensity. Obviously, in the latter case the distinction between ordinary and plasmon-type excitations cannot be based on oscillator strengths; here an alternative characterization is indispensable.

A. Computational methods

All calculations have been performed with the Q-Chem program package. The ground state minimum structures were obtained by geometry optimizations at the level of Møller-Plesset perturbation theory of second order (MP2)[66] using the augmented correlation consistent triple-ζ basis set aug-cc-pVTZ.[67] The excitation energies were obtained using different methods. At a more elementary level, RPA and CIS were used (taking into account both the Coulomb and exchange terms in the first-order electron-electron interaction). In addition, computations were performed using more accurate methods based on the second-order algebraic-diagrammatic construction (ADC(2)) approach.[68–73] The basis sets used in these computations were Dunning's cc-pVDZ or cc-pVTZ sets.[67]

In the ADC(2) computational schemes the excitation energies are obtained as eigenvalues of an hermitian secular matrix, the configuration space being spanned by singly (p-h) and doubly (2p-2h) excited configurations. In the p-h/p-h block of the secular matrix, the matrix elements derive from perturbation expansions extending through second order. As a result, the excitation energies of singly-excited states are treated consistently through second order. In the strict version, referred to as ADC(2)-s, doubly-excited states are treated in zeroth order, the 2p-2h/2p-2h block being a diagonal matrix

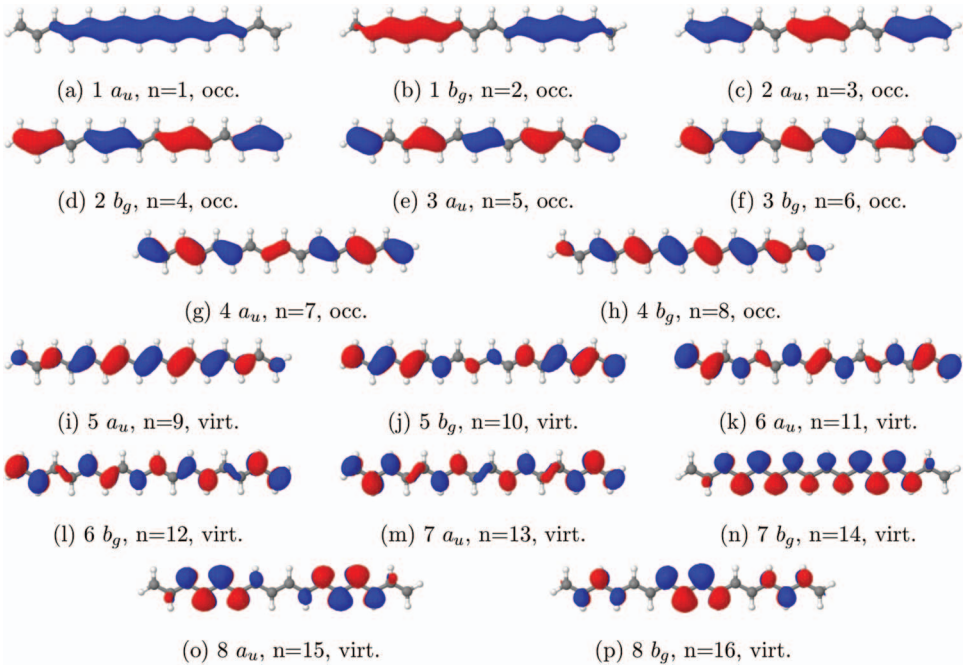

FIG. 3. Molecular orbitals of $C_{16}H_{18}$ and assignment of quantum numbers n.

TABLE I. Excitation energies, major p-h contributions to the eigenvectors, and oscillator strengths for the first excited states with B_u or A_g symmetry of octatetraene. The plasmon states are given in bold face. Methods: RPA/cc-pVTZ and CIS/cc-pVTZ. No contributions with an absolute amplitude larger than 0.3 (a weight larger than 9%) were omitted. Orbital numbering and relative signs as in Figure 2. Corresponding transition densities are shown in Figure 4.

	RPA					CIS				
		Major p-h contr.					Major p-h contr.			
State	Δ E[eV]	Orbital contr.	Δn	Amplitude	Osc. Str.	Δ E[eV]	Orbital contr.	Δn	Amplitude	Osc. Str.
1^1B_u	**4.58**	**4 → 5**	**1**	**0.9639**	**1.86**	**4.85**	**4 → 5**	**1**	**0.9595**	**1.91**
2^1A_g	**6.61**	**3 → 5**	**2**	**0.7456**	**...**	**7.05**	**3 → 5**	**2**	**0.7548**	**...**
		4 → 6	**2**	**0.6088**			**4 → 6**	**2**	**0.5762**	
3^1A_g	7.60	3 → 5	2	0.5990	...	7.65	3 → 5	2	0.5753	...
		4 → 6	2	−0.7281			4 → 6	2	−0.7464	
2^1B_u	**7.83**	**2 → 5**	**3**	**0.5267**	**0.09**	**8.25**	**2 → 5**	**3**	**0.3946**	**0.07**
		3 → 6	**3**	**0.4568**			**3 → 6**	**3**	**0.4165**	
		4 → 7	**3**	**0.6506**			**4 → 7**	**3**	**0.7392**	
3^1B_u	8.73	2 → 5	3	0.7138	0.01	8.79	2 → 5	3	0.7922	0.02
		3 → 6	3	|| < 0.2			3 → 6	3	0.1337	
		4 → 7	3	−0.6075			4 → 7	3	−0.4903	
4^1B_u	10.16	2 → 5	3	0.3012	0.15	10.30	2 → 5	3	0.2942	0.13
		3 → 6	3	−0.7354			3 → 6	3	−0.7511	
		4 → 7	3	|| < 0.2			4 → 7	3	0.1824	

of 2p-2h orbital energy differences. The computational cost of ADC(2)-s scales as N^5, where N is the number of basis functions.

An improved first-order treatment of the doubly-excited state is obtained at the extended ADC(2)-x level. Here the 2p-2h/2p-2h block is augmented by the first-order contributions taken from the third-order ADC(3) scheme. However, the computational cost of the ADC(2)-x treatment scales already as N^6. The better treatment of the doubly-excited states does not necessarily improve the results for single excitations. Often the mixing with doubly-excited states is overestimated, leading to too low excitation energies.[74] Recently, the scaled-opposite spin (SOS) approximation[75] was introduced in the ADC(2)-x scheme, leading to a semi-empirical SOS-ADC(2)-x variant[76] devised to cure the ADC(2)-x deficiencies.

In the attempts to identify plasmon-type states various characteristics have been addressed. Besides eigenvector structures, oscillator strengths (in the case of optically allowed transitions) and transition density patterns have been analyzed. As was realized by several authors (see, e.g., Refs. 37, 38, 51, 58, 59, 64, and 77), transition densities associated with plasmon excitations have an envelope with a specific nodal structure. In the plasmon-type excitations diagnosed via their scaling behavior, Bernadotte *et al.*[59] observed that the number of nodes in the transition density envelope correlates with the (energetic) order of the plasmons, the first having one node, the second two nodes, and so on.

B. Octatetraene

The assignment of wave vectors to the relevant frontier orbitals is shown for octatetraene in Figure 2. As an example, the three possible single-particle replacements with a quantum number change of three ($\Delta n = 3$) are shown. In the particle in a box model, they all correspond to the same momentum transfer, $q = 2\pi\,\Delta n/L = 6\pi/L$, and Δn is equal to the change in the number of nodes of the involved orbitals.

1. RPA and CIS results

Inspecting the excitation vectors obtained at the RPA level (Table I), it can be seen that the first state in B_u symmetry is dominated by the HOMO to LUMO transition ($\Delta n = 1$) while the next three states are mainly composed of single-particle replacements with $\Delta n = 3$. In the case of A_g symmetry, the first two states are dominated by transitions with $\Delta n = 2$.

This corresponds to the expectations based on the foregoing discussion. First of all, the excitations decouple to a large extent with respect to a given momentum transfer or Δn value. Furthermore, for $\Delta n = 1$ there exists one excited state while there are two for $\Delta n = 2$ and three for $\Delta n = 3$. In each Δn manifold, there is a distinguished state characterized as a coherent superposition of the elementary p-h excitations, each contributing with significant weight. For the lowest Δn values these particular states are 1^1B_u ($\Delta n = 1$), 2^1A_g ($\Delta n = 2$), and 2^1B_u ($\Delta n = 3$). They are clearly distinguished from the ordinary excitations, being composed of two or possibly three significant elementary excitations with differing relative phases, e.g., the 3^1B_u state in Table I. These characteristics allow us to refer to the distinguished excitations in each Δn manifold as plasmon-type excitations. Again, it is important to point out that the case $\Delta n = 1$ is special, because there is only one underlying single-particle replacement. Nevertheless, this case usually corresponds to the most intense excitation.

The corresponding transition densities are displayed in Figure 4. For the states identified as plasmons the envelopes of the transition densities show the expected nodal structure. For 1^1B_u ($\Delta n = 1$) the envelope of the transition density has one, for 2^1A_g ($\Delta n = 2$) two, and for 2^1B_u ($\Delta n = 3$) three nodes.

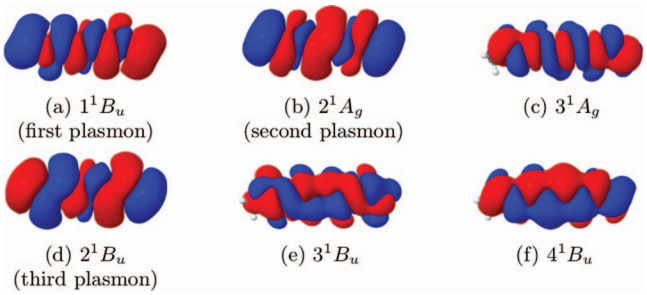

FIG. 4. Transition densities of octatetraene for the states of Table I (RPA/cc-pVTZ).

This nodal structure will become even more pronounced in the case of $C_{16}H_{18}$.

It should be noted, however, that the energies of the plasmon-type excitations are not always larger than the ordinary states within a given Δn manifold. A similar observation applies to the oscillator strengths. For example, the oscillator strength of the $\Delta n = 3$ plasmon (0.09) is lower than that of the 4^1B_u state (0.15), being the third state in the $\Delta n = 3$ manifold. Apparently, such deviations from the model behavior reflect the fact that the Coulomb contributions in the secular matrix modify the picture associated with a uniform interaction. Moreover, also the exchange contributions cannot be expected to be strictly uniform in the case of molecules. Nevertheless, the conditions for the emergence of plasmon-type excitations essentially apply to the polyene molecules considered here, as seen in the characteristic eigenvector structures and the transition density patterns.

The results of the simpler though related CIS method agree well with the RPA results (see Table I), and the analysis and identification of plasmon-type excitations is completely analogous. For the CIS transition densities, being very similar to those obtained at the RPA level, the reader is referred to the supplementary material.[62]

2. ADC(2) results

In view of the somewhat limited accuracy of the RPA (and CIS) approximations, it is of interest to test our findings in the outcome of the higher-order ADC(2)-s and SOS-ADC(2)-x methods. As discussed above, these methods treat single excitations consistently through second order perturbation theory while double excitations are described in zeroth and first order, respectively. For linear polyenes the inclusion of double excitations is known to play a crucial role.[74]

The ADC results are shown in Table II. As in the case of RPA, the states separate with respect to momentum transfer. Again, there is one state dominated by transitions with $\Delta n = 1$, two states with $\Delta n = 2$, and so on. Moreover, in each Δn group, there is a particular plasmon-type state formed as a coherent superposition of the elementary Δn excitations.

Interestingly, the order of the states has changed compared to RPA. Within the $\Delta n = 2$ manifold the plasmon-type

TABLE II. Excitation energies, major p-h contributions to the eigenvectors, oscillator strengths, and norm of double amplitudes for the first excited states with B_u or A_g symmetry of octatetraene. The plasmon states are given in bold face. Methods: ADC(2)-s/cc-pVTZ and SOS-ADC(2)-x/cc-pVTZ. No contributions with an absolute amplitude larger than 0.3 (a weight larger than 9%) were omitted. "n. c." stands for not calculated. Orbital numbering and relative signs as in Figure 2. Corresponding transition densities are shown in Figures 2 and 3 of the supplementary material.[62]

	ADC(2)-s					SOS-ADC(2)-x				
		Major p-h contr.		Norm			Major p-h contr.		Norm	
State	Δ E[eV]	Orbital contr.	Amplitude	2p-2h	Osc. Str.	Δ E[eV]	Orbital contr.	Amplitude	2p-2h	Osc. Str.
1^1B_u	**4.59**	**4 → 5**	**0.9438**	**0.08**	**1.69**	**4.91**	**4 → 5**	**0.9257**	**0.11**	**1.56**
2^1A_g	5.96	3 → 5	0.5058	0.13	…	4.47	3 → 5	0.4165	0.67	…
		4 → 6	−0.3796				4 → 6	−0.3452		
3^1A_g	n. c.					6.19	1 → 5	0.4893	0.46	…
							2 → 6	0.0919		
							3 → 7	−0.1034		
							4 → 8	−0.5011		
4^1A_g	**6.67**	**3 → 5**	**0.4080**	**0.08**	**…**	**6.88**	**3 → 5**	**0.6314**	**0.11**	**…**
		4 → 6	**0.5248**				**4 → 6**	**0.6643**		
2^1B_u	7.04	2 → 5	0.6589	0.13	0.00	5.60	2 → 5	0.4834	0.58	0.00
		3 → 6	−0.0402				3 → 6	|| < 0.02		
		4 → 7	−0.6129				4 → 7	−0.3874		
3^1B_u	n. c.					8.00	1 → 6	0.2779	0.76	0.00
							2 → 7	−0.0246		
							3 → 8	−0.3732		
4^1B_u	**7.99**	**2 → 5**	**0.6043**	**0.07**	**0.07**	**8.06**	**2 → 5**	**0.5042**	**0.13**	**0.05**
		3 → 6	**0.3499**				**3 → 6**	**0.3151**		
		4 → 7	**0.6293**				**4 → 7**	**0.6825**		
5^1B_u	8.71	2 → 5	0.2034	0.12	0.17	8.68	2 → 5	0.1397	0.32	0.10
		3 → 6	−0.8364				3 → 6	−0.7654		
		4 → 7	0.2502				4 → 7	0.1588		

TABLE III. Excitation energies, major p-h contributions to the eigenvectors, oscillator strengths, and norm of double amplitudes for the first excited states with B_u or A_g symmetry of $C_{16}H_{18}$. The plasmon states are given in bold face. Method: SOS-ADC(2)-x/cc-pVDZ. No contributions with an absolute amplitude larger than 0.3 (a weight larger than 9%) were omitted. Orbital numbering and relative signs as in Figure 3. Corresponding transition densities are shown in Figure 5.

		Major p-h contr.			Norm	
State	Δ E[eV]	Orbital contr.	Δn	Amplitude	2p-2h	Osc. Str.
2^1A_g	3.20	7 → 9	2	0.3356	0.70	…
		8 → 10	2	−0.3031		
1^1B_u	**3.75**	**8 → 9**	**1**	**0.9009**	**0.12**	**3.14**
2^1B_u	3.91	6 → 9	3	0.3859	0.70	0.00
		8 → 11	3	−0.3226		
3^1A_g	4.60	5 → 9	4	0.4035	0.65	…
		8 → 12	4	−0.3103		
4^1A_g	4.98	7 → 9	2	0.1832	0.88	…
		5 → 9	4	−0.1797		
		7 → 11	4	−0.1359		
5^1A_g	**5.10**	**7 → 9**	**2**	**0.6380**	**0.12**	**…**
		8 → 10	**2**	**0.6344**		
3^1B_u	5.23	4 → 9	5	0.4158	0.60	0.00
		5 → 10	5	0.2007		
		7 → 12	5	−0.1761		
		8 → 13	5	−0.3021		
4^1B_u	5.74	4 → 9	5	0.1056	0.88	0.00
		5 → 10	5	−0.1894		
		7 → 12	5	0.1517		
5^1B_u	6.10	2 → 9	7	0.4295	0.50	0.00
		3 → 10	7	0.2257		
		7 → 14	7	0.2066		
		8 → 15	7	−0.3601		
6^1B_u	**6.18**	**6 → 9**	**3**	**0.4517**	**0.14**	**0.31**
		7 → 10	**3**	**0.6415**		
		8 → 11	**3**	**0.4360**		

state is now highest in energy (as expected), while it ranks second in the $\Delta n = 3$ group. The intensities, however, are similar to the RPA and CIS results.

The transition densities of the plasmon-type states generated at the ADC(2) level are very similar to the RPA (or CIS) transition densities (see supplementary material[62]). As discussed above, the node pattern of the transition densities is consistent with the present eigenvector analysis.

The changes introduced by the transition from ADC(2)-s to SOS-ADC(2)-x are of special interest. First of all, states with higher Δn values are substantially lowered in energy and are now located energetically between the states considered so far (e.g., 5^1B_u and 3^1A_g in Table II). Moreover, the admixture of doubly excited configurations increase for all states except for the plasmon-type states. As a result, the plasmons are still dominated by single-particle transitions, whereas the ordinary states have increased double excitation character. The SOS-ADC(2)-x transition densities (see the supplementary material[62]) show the typical nodal patterns seen in the outcome of the other methods.

To summarize, the microscopic characteristics established at the RPA level of theory apply to the more accurate ADC(2) treatments as well.

C. $C_{16}H_{18}$

To apply the analysis also to a larger system, the longer $C_{16}H_{18}$ polyene was considered. In Figure 3, the Hartree-Fock π-orbitals are shown together with an assignment of wave vector quantum numbers n. The results obtained using the SOS-ADC(2)-x computational scheme and the cc-pVDZ basis set are listed in Table III. The choice of the SOS-ADC(2)-x method reflects the fact that low-lying double excitations play an important role in extended polyenes.

As an analysis of the eigenvectors shows, the separation with respect to momentum transfer or change in quantum number Δn is fulfilled to a large extent. Only in the case of the 4^1A_g state one finds single-particle contributions with differing Δn but similar weights. However, the latter state has strong 2p-2h character and is not comprised in the considered (p-h) model space.

Like in the SOS-ADC(2)-x results for octatetraene, most states show significant 2p-2h contributions, the exception

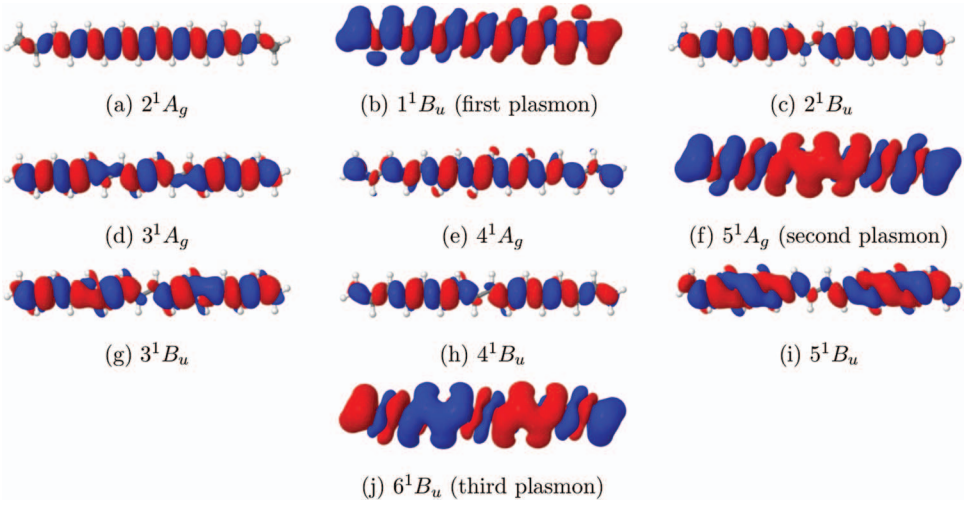

FIG. 5. Transition densities of $C_{16}H_{18}$ for the states of Table I as obtained with SOS-ADC(2)-x/cc-pVDZ.

being again the plasmon-type excitations. As to be expected, the oscillator strengths of the optically allowed plasmon-type transitions are larger than in octatetraene, reflecting the increased system size and the number of electrons participating in the "collective" excitations. It should be noted that the lowest ordinary B_u excitations have virtually vanishing oscillator strengths, so that the plasmon-type excitations will shape the optical spectrum in the low-energy region.

The transition densities are shown in Figure 5. Due to the extended system size the characteristic nodal structure of the transition densities' envelopes is easily recognizable, showing the typical nodal patterns for the states identified as plasmons by the eigenvector analysis. Consequently, the microscopic characteristics of plasmons in molecular systems derived above are also valid for this larger system.

IV. CONCLUSION

In this work, a microscopic characterization of plasmon-type excitations in molecules has been discussed. For this purpose, the RPA treatment of plasmon excitations in the electron gas was analyzed, allowing one to establish two basic characteristics: First, the secular (RPA) problem decouples with respect to momentum transfer so that the configuration space for a given momentum transfer is spanned by limited number of elementary p-h excitations; second, there is an essentially uniform interaction matrix owing to the predominant exchange contributions. As a result, there is a particular collective or plasmon-type solution, characterized as an equitable superposition of all elementary p-h excitations of the respective momentum transfer.

The conditions for the emergence of plasmon-type excitations could be validated in the case of two linear polyene molecules. Here the delocalized π-electrons can be viewed as constituting a quasi one-dimensional electron gas confined in a box. Assigning wave numbers (n) to the molecular π-orbitals, the approximate decoupling of states with differing momentum transfer (Δn values) could be retrieved in the final state eigenvectors. In particular, plasmon-type excitations could be identified as essentially equitable superpositions of the eligible elementary p-h excitations. The distinction of plasmon-type excitations and ordinary electron excitations based on the analysis of the final state eigenvectors worked both on the basic RPA/CIS and the higher ADC(2) levels of theory. The transition densities of states identified as being of plasmon-type showed the characteristic nodal structures addressed previously.

The concepts outlined here for linear polyenes should be transferable to non-linear molecular systems or nanoclusters provided an analogy can be established to a suitable electron gas model, e.g., electrons confined in a 2-d or 3-d box, a cylinder, or sphere. Such analogies have already been realized for a variety of systems for which plasmons are expected to be of great importance, e.g., acenes[51] or silver nanorods.[25] However, it is questionable whether this concept is transferable to systems which do not possess any (quasi-)symmetry at all.

ACKNOWLEDGMENTS

We thank S. Bernadotte for helpful discussions and bwGRiD[78] for providing computational resources. C.R.J. acknowledges funding from the DFG-Center for Functional Nanostructures at KIT.

[1] K. M. Mayer and J. H. Hafner, Chem. Rev. **111**, 3828 (2011).
[2] Y. Li, C. Jing, L. Zhang, and Y.-T. Long, Chem. Soc. Rev. **41**, 632 (2012).
[3] M. Swierczewska, G. Liu, S. Lee, and X. Chen, Chem. Soc. Rev. **41**, 2641 (2012).
[4] J. A. Schuller, E. S. Barnard, W. Cai, Y. C. Jun, J. S. White, and M. L. Brongersma, Nat. Mater. **9**, 193 (2010).
[5] H. A. Atwater and A. Polman, Nat. Mater. **9**, 205 (2010).
[6] H. J. Lezec, J. A. Dionne, and H. A. Atwater, Science **316**, 430 (2007).
[7] T. Ergin, N. Stenger, P. Brenner, J. B. Pendry, and M. Wegener, Science **328**, 337 (2010).
[8] A. Boltasseva and H. A. Atwater, Science **331**, 290 (2011).
[9] C. M. Soukoulis and M. Wegener, Nat. Photonics **5**, 523 (2011).
[10] W. Cai, J. S. White, and M. L. Brongersma, Nano Lett. **9**, 4403 (2009).
[11] A. Hryciw, Y. C. Jun, and M. L. Brongersma, Nat. Mater. **9**, 3 (2010).
[12] A. V. Akimov, A. Mukherjee, C. L. Yu, D. E. Chang, A. S. Zibrov, P. R. Hemmer, H. Park, and M. D. Lukin, Nature (London) **450**, 402 (2007).
[13] L. Tang, S. E. Kocabas, S. Latif, A. K. Okyay, D.-S. Ly-Gagnon, K. C. Saraswat, and D. A. B. Miller, Nat. Photonics **2**, 226 (2008).
[14] S. Linic, P. Christopher, and D. B. Ingram, Nat. Mater. **10**, 911 (2011).
[15] W. Hou, W. H. Hung, P. Pavaskar, A. Goeppert, M. Aykol, and S. B. Cronin, ACS Catal. **1**, 929 (2011).
[16] J. Lee, S. Mubeen, X. Ji, G. D. Stucky, and M. Moskovits, Nano Lett. **12**, 5014 (2012).
[17] S. Mukherjee, F. Libisch, N. Large, O. Neumann, L. V. Brown, J. Cheng, J. B. Lassiter, E. A. Carter, P. Nordlander, and N. J. Halas, Nano Lett. **13**, 240 (2013).
[18] D. Pines and D. Bohm, Phys. Rev. **85**, 338 (1952).
[19] D. Pines, Phys. Rev. **92**, 626 (1953).
[20] D. Bohm and D. Pines, Phys. Rev. **82**, 625 (1951).
[21] D. Bohm and D. Pines, Phys. Rev. **92**, 609 (1953).
[22] A. L. Fetter and J. D. Walecka, *Quantum Theory of Many-Particle Systems* (Dover Publications, Mineola, New York, 2003).
[23] S. M. Morton, D. W. Silverstein, and L. Jensen, Chem. Rev. **111**, 3962 (2011).
[24] C. M. Aikens, S. Li, and G. C. Schatz, J. Phys. Chem. C **112**, 11272 (2008).
[25] H. E. Johnson and C. M. Aikens, J. Phys. Chem. A **113**, 4445 (2009).
[26] N. Nayyar, V. Turkowski, and T. S. Rahman, Phys. Rev. Lett. **109**, 157404 (2012).
[27] G. F. Bertsch, A. Bulgac, D. Tománek, and Y. Wang, Phys. Rev. Lett. **67**, 2690 (1991).
[28] I. V. Hertel, H. Steger, J. de Vries, B. Weisser, C. Menzel, B. Kamke, and W. Kamke, Phys. Rev. Lett. **68**, 784 (1992).
[29] G. Gensterblum, J. J. Pireaux, P. A. Thiry, R. Caudano, J. P. Vigneron, P. Lambin, A. A. Lucas, and W. Krätschmer, Phys. Rev. Lett. **67**, 2171 (1991).
[30] A. Lucas, G. Gensterblum, J. J. Pireaux, P. A. Thiry, R. Caudano, J. P. Vigneron, P. Lambin, and W. Krätschmer, Phys. Rev. B **45**, 13694 (1992).
[31] E. Sohmen, J. Fink, and W. Krätschmer, Z. Phys. B **86**, 87 (1992).
[32] J. W. Keller and M. A. Coplan, Chem. Phys. Lett. **193**, 89 (1992).
[33] A. Manjavacas, F. Marchesin, S. Thongrattanasiri, P. Koval, P. Nordlander, D. Sánchez-Portal, and F. J. García de Abajo, ACS Nano **7**, 3635 (2013).
[34] W. A. de Heer, K. Selby, V. Kresin, J. Masui, M. Vollmer, A. Châtelain, and W. D. Knight, Phys. Rev. Lett. **59**, 1805 (1987).
[35] M. Koskinen, M. Manninen, and P. Lipas, Z. Phys. D **31**, 125 (1994).
[36] J.-P. Connerade and A. V. Solov'yov, Phys. Rev. A **66**, 013207 (2002).
[37] J. Yan, Z. Yuan, and S. Gao, Phys. Rev. Lett. **98**, 216602 (2007).
[38] J. Yan and S. Gao, Phys. Rev. B **78**, 235413 (2008).
[39] D. Gambacurta and F. Catara, J. Phys.: Conf. Ser. **168**, 012012 (2009).
[40] A. E. DePrince III, M. Pelton, J. R. Guest, and S. K. Gray, Phys. Rev. Lett. **107**, 196806 (2011).
[41] J. A. Scholl, A. L. Koh, and J. A. Dionne, Nature (London) **483**, 421 (2012).
[42] B. Gao, K. Ruud, and Y. Luo, J. Phys. Chem. C **118**, 13059 (2014).
[43] H. Weiss, R. Ahlrichs, and M. Häser, J. Chem. Phys. **99**, 1262 (1993).
[44] C. Yannouleas, E. N. Bogachek, and U. Landman, Phys. Rev. B **53**, 10225 (1996).
[45] R. Bauernschmitt, R. Ahlrichs, F. H. Hennrich, and M. M. Kappes, J. Am. Chem. Soc. **120**, 5052 (1998).

[46]R.-H. Xie, G. W. Bryant, G. Sun, M. C. Nicklaus, D. Heringer, T. Frauenheim, M. R. Manaa, Vedene H. Smith, Jr., Y. Araki, and O. Ito, J. Chem. Phys. **120**, 5133 (2004).
[47]T. L. J. Toivonen and T. I. Hukka, J. Phys. Chem. A **111**, 4821 (2007).
[48]A. Schlachter, Rev. Mex. Fís. S **56**, 30 (2010).
[49]P. Bolognesi, L. Avaldi, A. Ruocco, A. Verkhovtsev, A. Korol, and A. Solov'yov, Eur. Phys. J. D **66**, 254 (2012).
[50]A. Verkhovtsev, A. Korol, and A. Solov'yov, Eur. Phys. J. D **66**, 253 (2012).
[51]E. B. Guidez and C. M. Aikens, J. Phys. Chem. C **117**, 21466 (2013).
[52]E. B. Guidez and C. M. Aikens, Nanoscale **4**, 4190 (2012).
[53]E. Runge and E. K. U. Gross, Phys. Rev. Lett. **52**, 997 (1984).
[54]F. Furche, and D. Rappoport, in *Computational Photochemistry*, Theoretical and Computational Chemistry Vol. 16, edited by M. Olivucci (Elsevier, Amsterdam, 2005), Chap. III.
[55]A. Dreuw and M. Head-Gordon, Chem. Rev. **105**, 4009 (2005).
[56]V. Bonačić-Koutecký, P. Fantucci, and J. Koutecký, Chem. Rev. **91**, 1035 (1991).
[57]S. Kümmel and M. Brack, Phys. Rev. A **64**, 022506 (2001).
[58]S. Kümmel, K. Andrae, and P.-G. Reinhard, Appl. Phys. B **73**, 293 (2001).
[59]S. Bernadotte, F. Evers, and C. R. Jacob, J. Phys. Chem. C **117**, 1863 (2013).
[60]P. Ring and P. Schuck, *The Nuclear Many-body Problem* (Springer, New York, 1980).
[61]C. Kittel, *Introduction to Solid State Physics* (John Wiley & Sons, Inc., New York, 2005).
[62]See supplementary material at http://dx.doi.org/10.1063/1.4894266 for the discussion of further theoretical aspects as well as additional figures and coordinates of all minimum structures used in this work.
[63]J. E. del Bene, R. Ditchfield, and J. A. Pople, J. Chem. Phys. **55**, 2236 (1971).
[64]T. Yasuike, K. Nobusada, and M. Hayashi, Phys. Rev. A **83**, 013201 (2011).
[65]G.-T. Bae and C. M. Aikens, J. Phys. Chem. C **116**, 10356 (2012).
[66]C. Møller and M. S. Plesset, Phys. Rev. **46**, 618 (1934).
[67]T. H. Dunning, Jr., J. Chem. Phys. **90**, 1007 (1989).
[68]J. Schirmer, Phys. Rev. A **26**, 2395 (1982).
[69]J. Schirmer and A. B. Trofimov, J. Chem. Phys. **120**, 11449 (2004).
[70]A. B. Trofimov, G. Stelter, and J. Schirmer, J. Chem. Phys. **111**, 9982 (1999).
[71]A. B. Trofimov and J. Schirmer, J. Phys. B **28**, 2299 (1995).
[72]A. B. Trofimov, G. Stelter, and J. Schirmer, J. Chem. Phys. **117**, 6402 (2002).
[73]M. Wormit, D. R. Rehn, P. H. Harbach, J. Wenzel, C. M. Krauter, E. Epifanovsky, and A. Dreuw, Mol. Phys. **112**, 774 (2014).
[74]J. H. Starcke, M. Wormit, J. Schirmer, and A. Dreuw, Chem. Phys. **329**, 39 (2006).
[75]Y. Jung, R. C. Lochan, A. D. Dutoi, and M. Head-Gordon, J. Chem. Phys. **121**, 9793 (2004).
[76]C. M. Krauter, M. Pernpointner, and A. Dreuw, J. Chem. Phys. **138**, 044107 (2013).
[77]S. Malola, L. Lehtovaara, J. Enkovaara, and H. Häkkinen, ACS Nano **7**, 10263 (2013).
[78]See bwGRiD (http://www.bw-grid.de), member of the German D-Grid initiative, funded by the Ministry for Education and Research (Bundesministerium für Bildung und Forschung) and the Ministry for Science, Research and Arts Baden-Württemberg (Ministerium für Wissenschaft, Forschung und Kunst Baden-Württemberg).